

This work was written as part of one of the author's official duties as an Employee of the United States Government and is therefore a work of the United States Government. In accordance with 17 U.S.C. 105, no copyright protection is available for such works under U.S. Law. Access to this work was provided by the University of Maryland, Baltimore County (UMBC) ScholarWorks@UMBC digital repository on the Maryland Shared Open Access (MD-SOAR) platform.

Please provide feedback

Please support the ScholarWorks@UMBC repository by emailing scholarworks-group@umbc.edu and telling us what having access to this work means to you and why it's important to you. Thank you.

RESEARCH ARTICLE

10.1002/2016JD025331

Key Points:

- Box model-simulated glyoxal production from three isoprene oxidation mechanisms differ greatly
- Aerosol uptake of glyoxal was constrained using airborne in situ measurements and a global model
- Model results show that glyoxal contributes 0–14% of SOA in the Southeast U.S. during summer

Supporting Information:

- Supporting Information S1

Correspondence to:

J. Mao,
Jingqiu.Mao@noaa.gov

Citation:

Li, J., et al. (2016), Observational constraints on glyoxal production from isoprene oxidation and its contribution to organic aerosol over the Southeast United States, *J. Geophys. Res. Atmos.*, 121, 9849–9861, doi:10.1002/2016JD025331.

Received 9 MAY 2016

Accepted 29 JUL 2016

Accepted article online 31 JUL 2016

Published online 23 AUG 2016

Observational constraints on glyoxal production from isoprene oxidation and its contribution to organic aerosol over the Southeast United States

Jingyi Li¹, Jingqiu Mao^{1,2}, Kyung-Eun Min^{3,4,5}, Rebecca A. Washenfelder^{3,4}, Steven S. Brown^{3,6}, Jennifer Kaiser⁷, Frank N. Keutsch⁸, Rainer Volkamer^{4,6}, Glenn M. Wolfe^{9,10}, Thomas F. Hanisco¹⁰, Ilana B. Pollack^{3,4,11}, Thomas B. Ryerson³, Martin Graus^{3,4,12}, Jessica B. Gilman^{3,4}, Brian M. Lerner^{3,4}, Carsten Warneke^{3,4}, Joost A. de Gouw^{3,4}, Ann M. Middlebrook³, Jin Liao^{3,4}, André Welti^{3,4,13}, Barron H. Henderson¹⁴, V. Faye McNeill¹⁵, Samuel R. Hall¹⁶, Kirk Ullmann¹⁶, Leo J. Donner², Fabien Paulot^{1,2}, and Larry W. Horowitz²

¹Program in Atmospheric and Oceanic Sciences, Princeton University, Princeton, New Jersey, USA, ²Geophysical Fluid Dynamics Laboratory, National Oceanic and Atmospheric Administration, Princeton, New Jersey, USA, ³Chemical Sciences Division, NOAA Earth System Research Laboratory, Boulder, Colorado, USA, ⁴Cooperative Institute for Research in Environmental Sciences, University of Colorado, Boulder, Colorado, USA, ⁵Now at School of Environmental Science and Engineering, Gwangju Institute of Science and Technology, Gwangju, Korea, ⁶Department of Chemistry and Biochemistry, University of Colorado, Boulder, Colorado, USA, ⁷School of Engineering and Applied Sciences, Harvard University, Cambridge, Massachusetts, USA, ⁸School of Engineering and Applied Sciences and Department of Chemistry and Chemical Biology, Harvard University, Cambridge, Massachusetts, USA, ⁹Joint Center for Earth Systems Technology, University of Maryland Baltimore County, Baltimore, Maryland, USA, ¹⁰Atmospheric Chemistry and Dynamics Laboratory, NASA Goddard Space Flight Center, Greenbelt, Maryland, USA, ¹¹Now at Department of Atmospheric Science, Colorado State University, Fort Collins, Colorado, USA, ¹²Now at Institute of Atmospheric and Cryospheric Sciences, University of Innsbruck, Innsbruck, Austria, ¹³Now at Leibniz Institute for Tropospheric Research, Leipzig, Germany, ¹⁴Department of Environmental Engineering Sciences, Engineering School of Sustainable Infrastructure and Environment, University of Florida, Gainesville, Florida, USA, ¹⁵Department of Chemical Engineering, Columbia University, New York, New York, USA, ¹⁶Atmospheric Chemistry Observations and Modeling Laboratory, National Center for Atmospheric Research, Boulder, Colorado, USA

Abstract We use a 0-D photochemical box model and a 3-D global chemistry-climate model, combined with observations from the NOAA Southeast Nexus (SENEX) aircraft campaign, to understand the sources and sinks of glyoxal over the Southeast United States. Box model simulations suggest a large difference in glyoxal production among three isoprene oxidation mechanisms (AM3ST, AM3B, and Master Chemical Mechanism (MCM) v3.3.1). These mechanisms are then implemented into a 3-D global chemistry-climate model. Comparison with field observations shows that the average vertical profile of glyoxal is best reproduced by AM3ST with an effective reactive uptake coefficient γ_{glyx} of 2×10^{-3} and AM3B without heterogeneous loss of glyoxal. The two mechanisms lead to 0–0.8 $\mu\text{g m}^{-3}$ secondary organic aerosol (SOA) from glyoxal in the boundary layer of the Southeast U.S. in summer. We consider this to be the lower limit for the contribution of glyoxal to SOA, as other sources of glyoxal other than isoprene are not included in our model. In addition, we find that AM3B shows better agreement on both formaldehyde and the correlation between glyoxal and formaldehyde ($R_{\text{GF}} = [\text{GLYX}]/[\text{HCHO}]$), resulting from the suppression of δ -isoprene peroxy radicals. We also find that MCM v3.3.1 may underestimate glyoxal production from isoprene oxidation, in part due to an underestimated yield from the reaction of isoprene epoxydiol (IEPOX) peroxy radicals with HO_2 . Our work highlights that the gas-phase production of glyoxal represents a large uncertainty in quantifying its contribution to SOA.

1. Introduction

Glyoxal (CHOCHO) is one of the most abundant dicarbonyl compounds in the atmosphere. Its sources include direct emissions from biofuel use and biomass burning and secondary production from oxidation of various volatile organic compounds (VOCs) [Fu et al., 2008; Hays et al., 2002; Myriokefalitakis et al., 2008]. Glyoxal has a lifetime of about 1–3 h against photolysis and oxidation by OH at midday [Feierabend et al., 2009; Volkamer et al., 2005; Washenfelder et al., 2011]. It is highly water soluble, with a Henry's law constant of $3.0\text{--}4.2 \times 10^5 \text{ Matm}^{-1}$ at 298 K [Sander, 2015]. In aerosol water, the solubility increases rapidly at low salt concentrations (up to $5.0 \times 10^8 \text{ Matm}^{-1}$) [Kampf et al., 2013; Waxman et al.,

2015], due to the formation of glyoxal hydrate-sulfate complexes (“salting-in”) [Kurtén *et al.*, 2015]. However, this increase is inhibited at high salt concentrations by the kinetic limitation of gas-particle partitioning [Kampf *et al.*, 2013; Knote *et al.*, 2014]. Laboratory and field studies showed that glyoxal readily undergoes heterogeneous uptake to aerosols and cloud droplets to form secondary organic aerosol (SOA) [Carlton *et al.*, 2007; Ervens *et al.*, 2011; Galloway *et al.*, 2009, 2011b; Kroll *et al.*, 2005; Liggio *et al.*, 2005a, 2005b; Lim *et al.*, 2005; Volkamer *et al.*, 2007].

Glyoxal can provide important constraints on quantifying VOC emissions and oxidation mechanisms. Observations from aircraft, ground, and satellite show that glyoxal is often highly correlated with formaldehyde (HCHO), another product of VOC oxidation [Chan Miller *et al.*, 2014; DiGangi *et al.*, 2012; Kaiser *et al.*, 2015; MacDonald *et al.*, 2012; Chan Miller *et al.*, 2014; Stavrou *et al.*, 2009; Vrekoussis *et al.*, 2010]. The ratio of glyoxal to formaldehyde (surface or tropospheric column concentrations), R_{GF} , varies for different biogenic and anthropogenic VOC precursors, so it can be used to quantify the source strength of local VOC emissions [Chan Miller *et al.*, 2014; DiGangi *et al.*, 2012; Kaiser *et al.*, 2015; Chan Miller *et al.*, 2014; Vrekoussis *et al.*, 2010]. The NO_x ($\text{NO}_x = \text{NO} + \text{NO}_2$) dependence of R_{GF} , although it varies greatly for different VOCs, may offer additional information on VOC oxidation [DiGangi *et al.*, 2012; Kaiser *et al.*, 2015; Vrekoussis *et al.*, 2010]. Thus, it is important to evaluate model performance on R_{GF} and its NO_x dependence on regional and global scales, providing critical information for present and future satellite validation [Vrekoussis *et al.*, 2010].

Sources and sinks of glyoxal remain largely uncertain [Ervens *et al.*, 2011; Fu *et al.*, 2008; Galloway *et al.*, 2011a; Myriokefalitakis *et al.*, 2008; Stavrou *et al.*, 2009; Volkamer *et al.*, 2007; Washenfelder *et al.*, 2011]. Production from isoprene oxidation represents a major source of glyoxal on the global scale [Fu *et al.*, 2008]. Chamber experiments suggest a significant yield (up to 3%) of glyoxal from the first generation of isoprene oxidation under high NO_x conditions (500 ppbv NO) [Galloway *et al.*, 2011a; Volkamer *et al.*, 2006]. As we show below, this high yield may not reflect the distribution of β - and δ -isoprene peroxy radicals (ISOPO_2) as a function of their lifetimes under ambient conditions [Peeters *et al.*, 2014]. Another large uncertainty lies in the heterogeneous loss of glyoxal to aerosols and cloud droplets, which contributes to SOA mass. Laboratory studies indicate that the uptake of glyoxal depends on aerosol and cloud composition [Corrigan *et al.*, 2008; Jang *et al.*, 2002; Kroll *et al.*, 2005; Liggio *et al.*, 2005a, 2005b; Nozière *et al.*, 2009; Volkamer *et al.*, 2009; Waxman *et al.*, 2015], ambient relative humidity (RH) [Corrigan *et al.*, 2008; Hastings *et al.*, 2005; Kampf *et al.*, 2013; Liggio *et al.*, 2005a], and temperature [Gomez *et al.*, 2015]. By assuming irreversible reactive uptake with an uptake coefficient $\gamma_{\text{glyx}} = 2.9 \times 10^{-3}$, Fu *et al.* [2008] found that this process accounts for 14% of glyoxal loss globally. Volkamer *et al.* [2007] estimated γ_{glyx} of 3.7×10^{-3} in Mexico City, where glyoxal contributes about 15% of ambient SOA. A much lower γ_{glyx} ($0\text{--}8 \times 10^{-4}$ for the day and $(2 \pm 1) \times 10^{-4}$ for the night) was derived in Los Angeles [Washenfelder *et al.*, 2011], likely due to the high salt concentrations that kinetically limits glyoxal uptake [Kampf *et al.*, 2013; Knote *et al.*, 2014].

The Southeast Nexus (SENEX) aircraft campaign, which took place in June–July of 2013, aimed to improve the understanding of the interactions between biogenic and anthropogenic emissions over the Southeast U.S. It provided a detailed characterization of tropospheric photochemistry (gas and aerosol), including ozone, NO_y (NO , NO_2 , and its atmospheric oxidation products), biogenic VOCs (isoprene and monoterpenes), isoprene oxidation products, and organic aerosols [Warneke *et al.*, 2016]. In particular, glyoxal was measured on board the NOAA WP-3D aircraft using a cavity enhanced absorption spectroscopy technique [Min *et al.*, 2016], and formaldehyde was measured using laser-induced fluorescence technique [Cazorla *et al.*, 2015]. These measurements provide an unprecedented opportunity to examine the sources and sinks of glyoxal in this region, as well as its contribution to SOA mass.

Here we first examine the glyoxal yield from isoprene oxidation in a box model with three chemical mechanisms (AM3ST, AM3B, and the Master Chemical Mechanism (MCM) v3.3.1 [Jenkin *et al.*, 2015]). We then use field observations from the SENEX field campaign, interpreted with a chemistry-climate model, to understand the sources and sinks of glyoxal over the Southeast U.S. The comparison of the model to high-resolution aircraft data for both glyoxal and formaldehyde provides important new constraints on the potential for glyoxal to form SOA but also highlights uncertainty in the mechanism for isoprene oxidation, the single largest source of glyoxal in the Southeast U.S.

2. Methods

We apply a high-resolution ($50 \times 50 \text{ km}^2$) version of the Geophysical Fluid Dynamics Laboratory chemistry-climate model (GFDL AM3) to examine sources and sinks of glyoxal over the Southeast U.S. AM3 is the atmospheric component of the GFDL coupled model CM3. The dynamical core, physical parameterizations, cloud and precipitation processes, and cloud-aerosol interactions in AM3 are described in detail in *Donner et al.* [2011]. Chemistry in a previous version of AM3 has been described by *Naik et al.* [2013]. In this work, we nudge the horizontal wind field in the model toward values from the National Centers for Environmental Prediction Global Forecast System (NCEP GFS), allowing the model to simulate synoptic conditions corresponding to those sampled during field campaigns [*Lin et al.*, 2012]. We also apply finer vertical grids for convection plumes than the standard AM3 to improve the wet removal of tracers during summertime [*Paulot et al.*, 2016]. The photolysis module has been updated to FAST-JX v7.1 (<ftp://128.200.14.8/public/prather/Fast-J>) to compute the impacts from aerosols and clouds interactively. Dry deposition velocities prescribed in the model reflect rapid dry deposition of oxidized organic compounds [*Nguyen et al.*, 2015].

Biogenic emission of isoprene is computed using the Model of Emissions of Gases and Aerosols from Nature (MEGAN) inventory [*Guenther et al.*, 2006], with a total 15.9 Tg C in North America in June–August of 2013, which is slightly higher than previous estimates of 12.2–14.6 Tg C (June–August of 2006) in the same region [*Millet et al.*, 2008]. We reduce the isoprene emissions estimated by MEGAN by 20% (to 12.7 Tg C) to be consistent with other estimates of isoprene emission over the Southeast U.S. [*Warneke et al.*, 2010]. We do not consider glyoxal production from oxidation of monoterpenes and aromatics in this work, as their contribution is relatively small compared to isoprene over the Southeast U.S. [*Kaiser et al.*, 2015]. Inclusion of larger isoprene emissions and other VOC sources would proportionally increase the magnitude of glyoxal sinks derived in the analysis below. Anthropogenic emissions in 2013 follow the Representative Concentration Pathway 8.5 (RCP 8.5) projection [*Lamarque et al.*, 2011]. We applied diurnal variation anthropogenic NO_x emissions in North America following *Mao et al.* [2013b]. Anthropogenic NO_x emissions in RCP 8.5 are 0.34 Tg N/month over North America, comparable to the estimate from National Emissions Inventory (NEI) 2011 of 0.29 Tg N/month [*Travis et al.*, 2015]. We reduce these anthropogenic NO_x emissions by 25% to 0.26 Tg N/month to be consistent with recent estimates in this region [*Anderson et al.*, 2014].

2.1. Isoprene Chemistry

The standard isoprene mechanism used in AM3, “AM3ST,” is largely based on *Mao et al.* [2013b] following chamber observations from *Paulot et al.* [2009a, 2009b] and *Crouse et al.* [2011]. The main features of this mechanism include (1) substantial yield (7%) of first generation organic nitrates from δ -ISOPO₂, compared to 4.7% from β -ISOPO₂; (2) detailed assignment of the fate of first- and second-generation organic nitrates; and (3) isomerization of ISOPO₂ using the laboratory-determined rate constants. We further update this chemistry in several aspects. First, we assume a 25% molar yield of glyoxal from ISOPO₂ isomerization as the first-generation product [*Marais et al.*, 2016]. Second, the reaction of ISOPO₂ with HO₂ is updated following *St. Clair et al.* [2016a] to reflect a higher yield of unsaturated hydroxy hydroperoxides (ISOPOOH; 94%). Third, we adopt a new methylvinyl ketone (MVK) oxidation chemistry in which the glycolaldehyde molar yield is increased from 0.53 to 0.72 under high NO_x conditions [*Praske et al.*, 2015]. Fourth, we include fast photolysis of carbonyl organic nitrates [*Müller et al.*, 2014]. Fifth, we adopt a substantially slower ozonolysis rate of isoprene β -hydroxy nitrate (ISOPNB; $3.7 \times 10^{-19} \text{ molecule}^{-1} \text{ cm}^3 \text{ s}^{-1}$ [*Lee et al.*, 2014]) than the previous value from *Lockwood et al.* [2010] ($1.06 \times 10^{-16} \text{ molecule}^{-1} \text{ cm}^3 \text{ s}^{-1}$). Lastly, we update the NO_3 -initiated chemistry of isoprene following MCM v3.2 [*Jenkin et al.*, 1997; *Saunders et al.*, 2003]. As illustrated in Figure S1 in the supporting information, glyoxal is produced in the first generation of isoprene oxidation, both from the decomposition of alkoxy radical (DIBOO shown in Figure S1) through the δ -channel under high NO_x conditions [*Peeters and Nguyen*, 2012] and from isomerization of ISOPO₂ under low NO_x conditions [*Stavrakou et al.*, 2010]. Glyoxal is further produced in later generations from oxidation of carbonyl compounds including glycolaldehyde and isoprene epoxydiol (IEPOX).

In this work, we introduce an additional mechanism, “AM3_beta” (AM3B), to reflect more recent updates to the understanding of isoprene oxidation. Both theoretical and experimental studies indicate that β - and δ -ISOPO₂ undergo fast interconversion [*Bates et al.*, 2014; *Crouse et al.*, 2011; *Peeters et al.*, 2014]. One important implication is that oxidation products observed in experimental chambers at ~ 500 ppbv NO may not

reflect the products in ambient air, where NO is several orders of magnitude lower. This is due to a higher fraction of δ -ISOPO₂ loss via bimolecular reactions than interconversion back to β -ISOPO₂ under high NO_x conditions. To reflect this change, we only allow β -ISOPO₂ to react with NO because δ -ISOPO₂ is believed to only account for <3% of total ISOPO₂ under ambient conditions [Peeters *et al.*, 2014]. The yield of β -hydroxyl isoprene nitrate (ISOPNB) is assumed to be 0.1, an average of the suggested values 0.09 [Xiong *et al.*, 2015] and 0.16 [Teng *et al.*, 2015]. The yields of HCHO, MVK, and methacrolein (MACR) from β -ISOPO₂ + NO are adjusted accordingly for carbon balance. As we show below, this update changes the production of formaldehyde and glyoxal under high NO_x conditions.

The Leeds Master Chemical Mechanism (MCM) is a near-explicit chemical mechanism that describes gas-phase VOC chemistry. The latest revision, v3.3.1, includes recent updates for OH-initiated isoprene chemistry [Jenkin *et al.*, 2015], such as isoprene-peroxy radical interconversion and isomerization pathways [Peeters *et al.*, 2014], and the chemistry of IEPOX [Bates *et al.*, 2014; Paulot *et al.*, 2009b]. Consequently, these updates show significant differences in simulated HO_x (HO_x = OH + HO₂), NO_x, and major oxidation products compared to earlier versions of MCM. To evaluate the performance of MCM v3.3.1 in our global model, we implement a MCM-like mechanism ("AM3M") by adjusting the production of glyoxal from major pathways in the AM3B mechanism to approximate the glyoxal and HCHO yields of MCM v3.3.1 in a highly condensed chemical mechanism suitable for use in a global model (Figure S2).

2.2. Heterogeneous Loss of Glyoxal

Heterogeneous loss onto aerosols and cloud droplets plays an important role in the fate of dicarbonyls. Here we assume that this process is irreversible and can be represented by a first-order reactive uptake rate constant k [Mao *et al.*, 2010]

$$k = \left(\frac{a}{D_g} + \frac{4}{v\gamma} \right)^{-1} A$$

where a is the effective radius of aerosols or cloud droplets, D_g is the gas phase diffusion constant, γ is the reactive uptake coefficient, A is the surface area of aerosols or cloud droplets, and v is the mean molecular velocity of the gas molecule.

We allow this process to take place on five types of aerosols including sulfate, black carbon, primary organic carbon, sea salt, mineral dust, and SOA, with hygroscopic growth included [Mao *et al.*, 2013a]. Given the large uncertainties associated with the uptake of glyoxal, we use field observations to assess the possible range of γ_{glyx} . We do not include glyoxal uptake by cloud droplets in this work, because the uptake coefficient by aerosols is much greater and because large uncertainties are associated with mixing of cloudy and no-cloud volumes within a grid box [Huijnen *et al.*, 2014; Jacob, 2000]. We include heterogeneous loss of methylglyoxal with an uptake coefficient of 7.6×10^{-3} [Zhao *et al.*, 2006] to produce better closure with total organic aerosol in the model.

The irreversible surface uptake coefficient, γ_{glyx} , applied here should be viewed as an "effective reactive uptake coefficient" to simply represent the net heterogeneous loss of glyoxal that does not revert back to the gas phase and provide an estimate for its contribution to SOA mass on the regional scale. Previous studies have indicated that this process is likely reversible to some extent [Galloway *et al.*, 2009; Kroll *et al.*, 2005]. We show below that the values of γ_{glyx} are dependent on the choice of gas-phase chemistry.

3. NO_x-Dependent Glyoxal and HCHO Yields

We first conduct box model simulations to quantify the yield of glyoxal and HCHO from isoprene oxidation as a function of NO_x levels, using the Dynamically Simple Model of Atmospheric Chemical Complexity (DSMACC) [Emmerson and Evans, 2009]. We test three mechanisms (AM3ST, AM3B, and MCM v3.3.1) in the model. The model is initialized at 8:00 local time for midlatitude summer conditions, with 1 ppbv of isoprene; 60 ppbv of ozone; 150 ppbv of CO; and a choice of 0.01, 0.1, or 1 ppbv of NO_x. While NO_x is held constant, isoprene is allowed to decay over time. Figure 1 shows the cumulative yields of glyoxal and HCHO per unit carbon from isoprene oxidation at various NO_x levels after 3 days of model integration with their loss processes turned off [Palmer *et al.*, 2003]. We also use tagged tracers for individual pathways (β / δ -ISOPO₂ + NO, ISOPO₂ + HO₂, and isomerization of ISOPO₂) to compute their contribution in each mechanism.

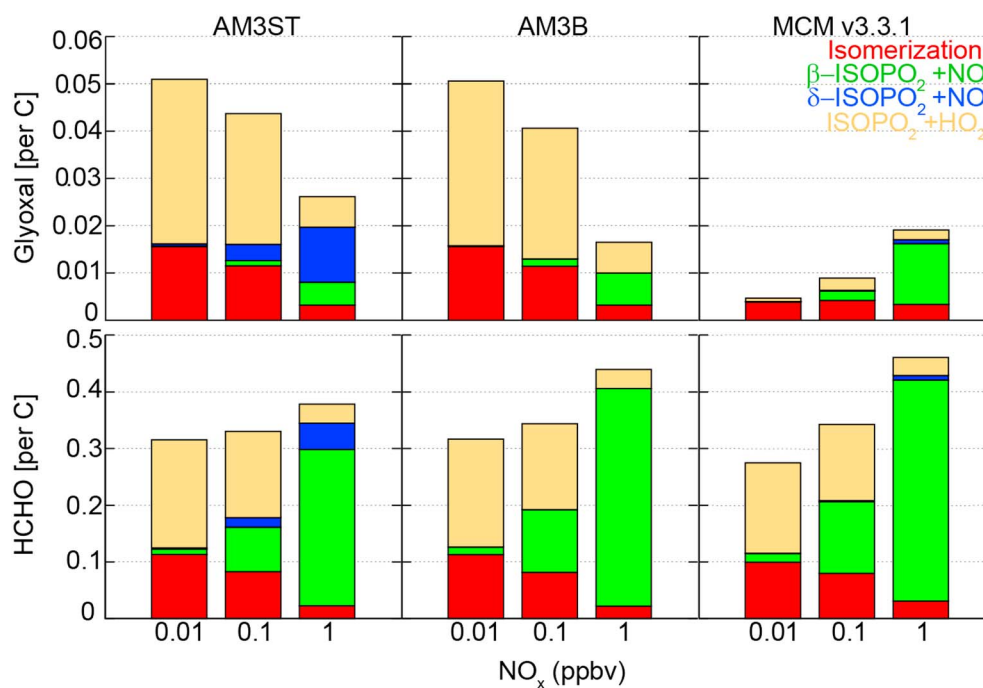


Figure 1. Cumulative yields of glyoxal and HCHO in major pathways from isoprene oxidation at different NO_x levels. Glyoxal and HCHO from isoprene oxidized by O₃ and by NO₃ are not shown due to low production in all the mechanisms.

A striking difference between the MCM v3.3.1 and AM3 mechanisms is the glyoxal production under low NO_x conditions. While the AM3 mechanisms show a large yield of glyoxal from isomerization of ISOPO₂ and the oxidation of IEPOX (via the ISOPO₂ + HO₂ pathway), MCM v3.3.1 shows very little production of glyoxal from these channels. For the isomerization pathway, MCM v3.3.1 assumes that 50% of 1,6-H shift isomerization flux produces hydroperoxyaldehydes (HPALDs), with another 50% produces complex dihydroperoxy formyl peroxy radicals, referred as “di-HPCARPs” by *Peeters et al.* [2014]. MCM v3.3.1 includes low production of glyoxal from the degradation of HPALDs and di-HPCARPs. On the other hand, the AM3 mechanisms do not include di-HPCARPs and assume fast photolysis as the only loss process of HPALDs, with prompt yield of glyoxal following *Stavrakou et al.* [2010].

Another large difference in glyoxal yield comes from the treatment of the ISOPO₂ + HO₂ pathway, particularly regarding the fate of IEPOX. MCM v3.3.1 assumes major production of organic peroxides from the reaction of IEPOX peroxy radicals (IEPOXOO; α -carbonyl peroxy radicals) with HO₂, while AM3 mechanisms follow *Paulot et al.* [2009b] and assume full radical propagation for this reaction, with a 28% yield of glyoxal. As a result, a much higher yield of glyoxal is predicted from the ISOPO₂ + HO₂ pathway in the AM3 mechanisms compared to MCM v3.3.1. In fact, several studies have confirmed significant OH production from the reaction of HO₂ with α -carbonyl peroxy radicals [*Dillon and Crowley*, 2008; *Hasson et al.*, 2004; *Jenkin et al.*, 2007]. This is also consistent with recent studies of IEPOX kinetics, which show very little formation of peroxides under low NO_x conditions [*Bates et al.*, 2014; *Jacobs et al.*, 2013].

Under high NO_x conditions, the three mechanisms show better agreement for glyoxal production, though with different pathways contributing. MCM v3.3.1 shows dominant production from the β -ISOPO₂ + NO pathway, mainly due to a higher yield of glyoxal from oxidation of glycolaldehyde (20%), based on *Niki et al.* [1987]. An even higher yield of glyoxal (29%) was adopted by *Galloway et al.* [2011a]. In contrast, the AM3 mechanisms apply a lower yield of glyoxal (13%) following *Butkovskaya et al.* [2006]. Surprisingly, both AM3ST and AM3B show significant production from isomerization of ISOPO₂ and the ISOPO₂ + HO₂ pathway, suggesting the potential importance of these channels for glyoxal production even under high NO_x conditions. AM3ST has major production from the δ -ISOPO₂ + NO pathway, leading to 60% higher glyoxal yield than AM3B. MCM v3.3.1 shows a small contribution from the δ -ISOPO₂ + NO channel, due to a small fraction of δ -ISOPO₂ in the radical pool of ISOPO₂ (<3%). This reflects a different distribution of δ -ISOPO₂ and

β -ISOPO₂ under ambient conditions versus very high NO chamber conditions [Peeters *et al.*, 2014], consistent with our assumption in AM3B. Overall, the AM3 mechanisms show decreasing glyoxal production with increasing NO_x concentration, whereas MCM v3.3.1 shows the opposite.

The HCHO yield and its NO_x dependence appear to be more consistent across the different mechanisms. Under low NO_x conditions, isomerization of ISOPO₂ and the ISOPO₂ + HO₂ pathway contribute most to HCHO. At NO_x = 1 ppbv, the ISOPO₂ + NO pathway becomes the primary source of HCHO. The HCHO yield in AM3B is 17% higher than AM3ST and comparable to MCM v3.3.1, mainly due to a higher HCHO yield from the β -ISOPO₂ + NO pathway than the δ -ISOPO₂ + NO pathway. It should be noted that the cumulative yields shown in Figure 1 represent the potential glyoxal and HCHO produced from sufficient oxidation of 1 ppbv isoprene and the intermediate VOCs. This is different from ambient conditions that isoprene is continuously emitted and the production of glyoxal and HCHO are dependent on OH levels (i.e., the production rate of ISOPO₂). Chemical loss of HCHO and glyoxal are similar across the mechanisms (Table S1 in the supporting information).

The NO_x-dependent yields of glyoxal and HCHO from box model results are useful to identify their major production pathways at different NO_x levels. This knowledge can be translated to 3-D model output and help evaluate model performance from these pathways using aircraft observations.

4. Observational Constrains on Glyoxal Production

4.1. Vertical Profiles of Gaseous and Particulate Species

We compare the AM3 model predictions for glyoxal, formaldehyde, and isoprene oxidation products to measurements of these species acquired during the SENEX field campaign. All measurements are averaged to 1 min time resolution. The measurement accuracies for isoprene, formaldehyde, NO_x, glyoxal, organic aerosol, and aerosol surface area are 25%, 10%, 5%, 5.8%, 50%, and 36%, respectively [Warneke *et al.*, 2016, and the references therein]. Although other carbonyl compounds have recently been found to suffer from inlet artifacts arising from catalytic conversion of organic hydroperoxides on metal inlet surfaces [Rivera-Rios *et al.*, 2014], we do not expect such interferences for glyoxal since no metal surfaces are present in the glyoxal sampling line [Min *et al.*, 2016] and since there are currently no known mechanisms for conversion of hydroperoxides to glyoxal. We also expect little interferences for formaldehyde since its residence time during exposure to metal surfaces is very small [Cazorla *et al.*, 2015]. This is confirmed by recent laboratory tests, suggesting that the interference is <5% for this specific instrument [St. Clair *et al.*, 2016b]. We exclude biomass burning, urban plumes, stratospheric air (CH₃CN \geq 225 pptv, NO_x/NO_y > 0.4 or NO₂ > 4 ppbv, and O₃/CO > 1.25 mol/mol, respectively) from our analysis following Hudman *et al.* [2007], and omit data from the Ozark Mountains, where the model shows a significant positive bias for isoprene (Figure S3). We also exclude nighttime flights from our analysis.

Figure 2 shows the mean vertical profiles of observed and modeled isoprene, glyoxal, HCHO, and other related species during SENEX. Model output is sampled along the flight tracks and at the flight time with 1 h time resolution. We include two model simulations (AM3ST and AM3B). MCM v3.3.1 is not included because of its complexity. Instead, we show AM3M in our global model as a proxy to MCM v3.3.1 in the following sections. Simulated NO_x agrees with the observations at all altitudes except for a slight overestimate (~20%) near the surface. Observed isoprene concentration peaks near the surface at 1.2 ppbv and decreases gradually with altitude. Both AM3ST and AM3B show a positive bias of isoprene below 1 km, but no such bias is evident for HCHO. As HCHO in this region is dominantly produced from isoprene and has a relatively longer lifetime than that of isoprene (4 h versus <1 h), we attribute this positive bias of modeled isoprene partly to sampling bias and partly to shallow boundary layer and slow vertical mixing in the current model. We further examine modeled OH and J values using ICARTT [Mao *et al.*, 2013b] and NOMADSS (https://www.eol.ucar.edu/field_projects/nomadss) field observations over the eastern U.S., and we find that the model agrees with observed OH and J values within 20% (Figures S4 and S5).

Like isoprene, both HCHO and glyoxal decrease with altitude, reflecting their short photochemical lifetimes (4 h and 3.5 h) and their dominant source from isoprene. In particular, the observed vertical profiles of glyoxal and HCHO appear to be in remarkable agreement with previous observations collected in the same region during the 1995 Nashville/Middle Tennessee Ozone Study [Lee *et al.*, 1998]. Our model is able to reproduce

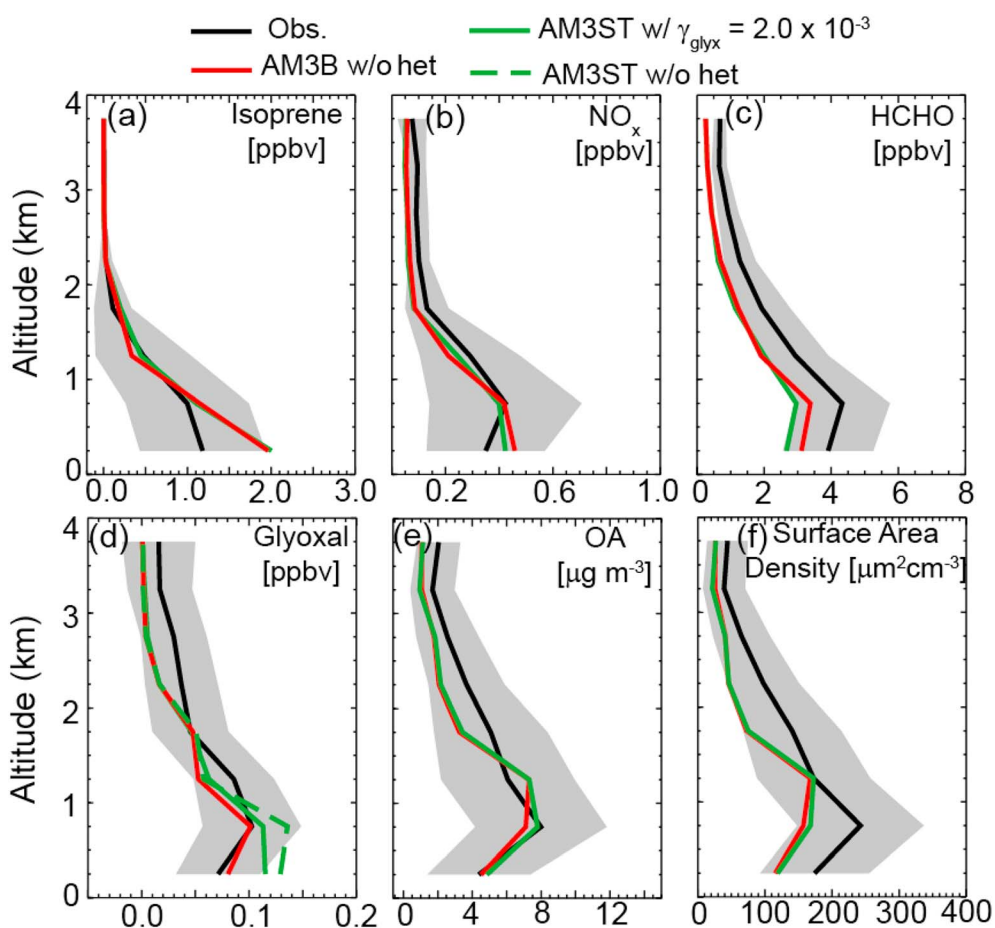


Figure 2. Mean vertical profiles of isoprene, HCHO, NO_x , glyoxal, organic aerosol (OA), and surface area density of aerosol during SENEX. The grey shades are the standard deviation (σ) of the averaged profiles of the measured tracers. The dashed green line in Figure 2d is the model estimate without heterogeneous loss of glyoxal by AM3ST. Observed organic aerosol mass and aerosol surface area density are from dry particles.

their vertical gradients, although the vertical profiles of HCHO and glyoxal appear to be sensitive to the choice of photochemical mechanisms. AM3ST underestimates HCHO by 32% and overestimates glyoxal almost by a factor of 2 near the surface. With the suppression of $\delta\text{-ISOPO}_2$ in AM3B, HCHO is increased by 17% and glyoxal is decreased by 38% near the surface, leading to better agreement with observations for both species.

The abundance of glyoxal is also dependent on its heterogeneous loss. By assuming an irreversible reactive uptake on aerosols, an optimal value of γ_{glyx} is selected to minimize the difference between modeled and observed glyoxal in the boundary layer. We find that the best agreement is achieved for AM3ST with γ_{glyx} of 2×10^{-3} and for AM3B with γ_{glyx} of 0 (Table S2); we adopt those values in the following analysis.

The γ_{glyx} derived with AM3B is lower than the value from previous laboratory experiments (2.9×10^{-3} by Liggio *et al.* [2005b]), likely due to three reasons. First, there could be a missing source of gas-phase glyoxal in the current mechanism, which can be compensated by aerosol uptake and lead to a higher contribution to SOA formation. We find that a 30% increase in glyoxal production in AM3B would be required to approximately compensate aerosol uptake of glyoxal with $\gamma_{\text{glyx}} = 2.9 \times 10^{-3}$. Second, there are other sources other than isoprene oxidation that could contribute to production of glyoxal but are not included in the current model, such as oxidation of anthropogenic VOCs and monoterpenes. Field observations show glyoxal in the transition layer above biogenic VOC hot spots in the Southeast U.S. [Lee *et al.*, 1998], anthropogenic and biogenic VOC hot spots during California Nexus (CalNex) [Baidar *et al.*, 2013], and in remote air [Volkamer *et al.*, 2015] that still remain unexplained and would lead to a higher uptake coefficient in our

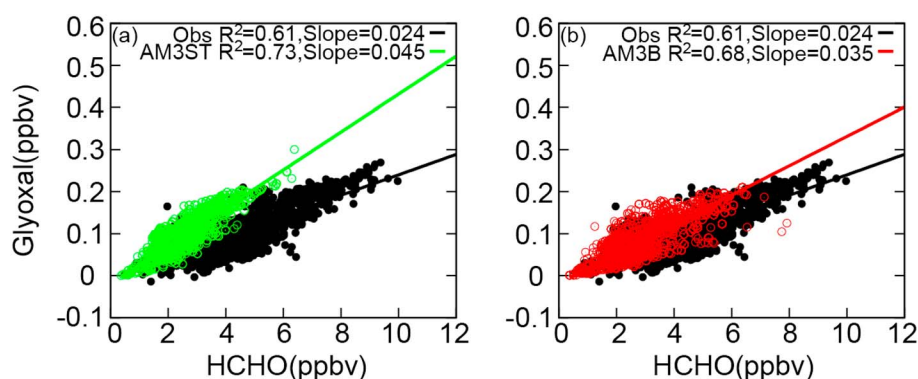


Figure 3. Correlation between glyoxal and HCHO below 1.5 km during SENEX. The black dots represent the observations, while the green and red open circles show the (left) AM3ST with $\gamma_{\text{glyx}} = 2.0 \times 10^{-3}$ and (right) AM3B without heterogeneous loss of glyoxal. The solid lines are the linear regression lines, with regression slopes calculated from least squares fits.

estimate. Third, the effective aerosol uptake coefficient, as we assumed here to represent the net heterogeneous loss of glyoxal, is indeed smaller than the value from the previous studies. One possibility is that the aerosol uptake of glyoxal is to some extent reversible [Galloway *et al.*, 2009; Kroll *et al.*, 2005], which would lead to a lower estimate of γ_{glyx} . Another possibility is the suppression of glyoxal loss to ambient aerosols containing organic and inorganic components, resulting from its organic coating [Ciobanu *et al.*, 2009; Galloway *et al.*, 2011b; Gaston *et al.*, 2014]. It is also possible that additional production of glyoxal in the particle phase from other organic compounds reduces the net loss of glyoxal to the aerosol surface.

Overall, the resulting average contribution of glyoxal to organic aerosols is about $0.8 \mu\text{g m}^{-3}$ for AM3ST (Figure S7) and negligible for AM3B in the boundary layer over the Southeast U.S. We emphasize that this is likely the lower limit of glyoxal SOA, as other glyoxal sources such as anthropogenic VOCs and monoterpenes are not included in our model. Accounting for these additional sources would require a higher sink of glyoxal and therefore results in higher glyoxal SOA. The estimate from AM3ST is comparable to previous model studies over the same region, assuming reversible or irreversible reactive uptake of glyoxal onto aerosols [Knote *et al.*, 2014; Li *et al.*, 2015; Ying *et al.*, 2015], while AM3B is not. We also find that the inclusion of IEPOX aerosol uptake may reduce glyoxal in the boundary layer by less than 15% over the Southeast U.S. (Figure S8). This would lead to an even lower estimate of glyoxal SOA.

4.2. R_{GF} and Its Dependence on NO_x

Comparison of modeled and observed R_{GF} provides additional constraint on the gas-phase chemistry for glyoxal production. Figure 3 shows the covariation of glyoxal and formaldehyde in the boundary layer during SENEX. The linear regression slope (R_{GF}) derived from observations is 2.4% ($R^2 = 0.61$) in the boundary layer over the Southeast U.S., suggesting that the dominant source of both glyoxal and formaldehyde in this region is isoprene [Kaiser *et al.*, 2015]. The AM3ST mechanism overestimates R_{GF} by a factor of 2, while better agreement is achieved by the AM3B mechanism, due to the suppressed production of glyoxal and enhanced production of HCHO. Simulations with both mechanisms significantly underestimate the range of HCHO concentrations observed. Without heterogeneous loss of glyoxal, the model with AM3ST significantly overestimates R_{GF} but predicts a similar result as assuming no heterogeneous loss of glyoxal with AM3B.

We further examine the NO_x dependence of HCHO, glyoxal, and R_{GF} during SENEX (Figure 4). A prominent feature of Figure 4 is the high similarity between the observed NO_x dependence of HCHO and glyoxal. Both HCHO and glyoxal are observed to increase with NO_x concentrations and to start to level off at 1 ppbv of NO_x . Remarkably, R_{GF} shows little variation across NO_x concentrations, consistent with Kaiser *et al.* [2015]. Both AM3ST and AM3B are able to reproduce the NO_x dependence of HCHO, although they tend to underestimate HCHO by 1–2 ppbv across NO_x regimes, consistent with Wolfe *et al.* [2016]. AM3B shows better agreement with observations than AM3ST at high NO_x level, indicating that δ -channel is suppressed under ambient conditions. Using the optimized γ_{glyx} values described above (2×10^{-3} for AM3ST and 0 for AM3B), our model can roughly capture the NO_x dependence of glyoxal. In contrast to Figure 1, neither

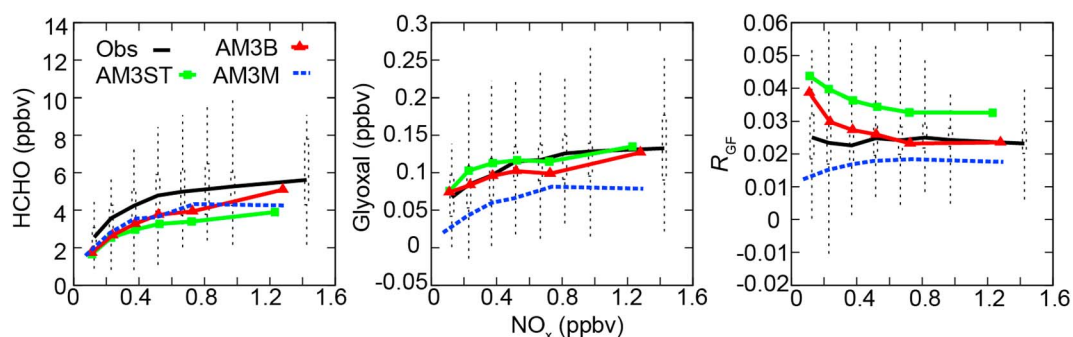


Figure 4. HCHO (ppbv), glyoxal (ppbv), and R_{GF} in each NO_x bin below 1.5 km during SENEX. The dots, dashed boxes, and whiskers are the mean, interquartile range, and lowest and highest of the observations; the green squares and red triangles are the mean of AM3ST with $\gamma_{glyx} = 2.0 \times 10^{-3}$ and AM3B without heterogeneous loss of glyoxal, respectively; and the blue dashed lines are the mean of AM3M without heterogeneous loss of glyoxal.

AM3ST nor AM3B shows high glyoxal concentrations under low NO_x conditions, reflecting slower production of glyoxal under such conditions due to low OH radical concentrations and slow $ISOPO_2$ production rate in the ambient atmosphere [Wolfe et al., 2016]. Although the NO_x -dependent HCHO and glyoxal are individually captured qualitatively, a large positive bias in R_{GF} is apparent for AM3ST across NO_x regimes and for AM3B at $NO_x < 0.5$ ppbv. We attribute the bias in AM3ST to the overestimate of glyoxal under low NO_x and underestimate of HCHO across NO_x regimes. The bias in AM3B is mainly due to the underestimate of HCHO.

To examine the NO_x dependence of HCHO, glyoxal, and R_{GF} from MCM v3.3.1, the AM3M mechanism that mimics MCM v3.3.1 is then tested in our AM3 global model. Comparison to the SENEX data (Figure 4) shows that AM3M can also well reproduce the NO_x dependence of HCHO, similar to the performance of other AM3 mechanisms. However, AM3M largely underestimates glyoxal and R_{GF} across all NO_x levels, suggesting additional sources of glyoxal needed in the current MCM mechanism. Inclusion of heterogeneous loss of glyoxal would further reduce glyoxal in AM3M and worsen the comparison. One possible reason for the underestimate of glyoxal in AM3M is the lack of a radical propagating channel for the $IEPOXOO + HO_2$ reaction in MCM v3.3.1, as described above.

R_{GF} provides a useful tool to estimate global production of glyoxal from isoprene oxidation. In particular, the fact that R_{GF} is insensitive to NO_x allows us to directly compute its global production rate. Assuming 0.4 HCHO yield per isoprene C (Figure 1; also consistent with Palmer et al. [2003]) and a global constant R_{GF} of 2.4% (according to the measurements during SENEX), we can derive the global production of 23 Tg glyoxal with 500 Tg isoprene emitted annually [Guenther et al., 2006]. This is similar to a previous estimate of 21 $Tg\ yr^{-1}$ glyoxal from isoprene [Fu et al., 2008].

5. Budget of Glyoxal in North America

Table 1 summarizes the monthly averaged glyoxal budget over North America (20~55°N, 60~130°W) in the boundary layer (0–1.5 km) during June–July of 2013 for AM3ST and AM3B. The total chemical production

Table 1. Budget of Glyoxal over North America (20~55°N, 60~130°W) Below 1.5 km in June–July of 2013 ^a		
	AM3ST	AM3B
$\gamma_{glyx} (\times 10^{-3})$	2.0	0
Production (Tg/month)	0.44	0.32
Chemical loss (Tg/month)	0.41	0.29
Photolysis	57%	77%
OH	17%	23%
Uptake by aerosols	26%	-
Dry deposition (Tg/month)	1.2×10^{-2}	1.2×10^{-2}
Wet deposition (Tg/month)	1.1×10^{-2}	1.6×10^{-2}

^aPercentage is the contribution of each pathway to the total chemical loss of glyoxal.

of glyoxal varies with the chemical mechanisms, from 0.32 Tg/month with AM3B to 0.44 Tg/month with AM3ST. The major sink of glyoxal with both mechanisms is photolysis, followed by aerosol uptake and OH oxidation for AM3ST and OH oxidation and aerosol uptake for AM3B, although the contribution of each pathway varies with mechanisms and γ_{glyx} . For example, in AM3ST, heterogeneous loss is an important sink, accounting for 26% of the total chemical loss of glyoxal; however, the contribution is negligible in the AM3B simulations. Deposition accounts for 5–9% of total glyoxal loss in the model. We show in this work that the estimates of sources and sinks of glyoxal are dependent on the choice of gas-phase chemistry.

6. Conclusions and Discussion

A 0-D photochemical box model and a 3-D chemistry-climate model applied to data from the Southeast U.S. during the SENEX field campaign provide the first model evaluation of in situ glyoxal aircraft observations.

We find that the three mechanisms (AM3ST, AM3B, and MCM v3.3.1) show similarity in HCHO but large differences in glyoxal, leading to opposite NO_x dependence of R_{GF} . Under low NO_x conditions, the AM3 mechanisms predict much higher glyoxal yields than MCM v3.3.1, largely due to the significant contribution from isomerization of ISOPO_2 and oxidation of IEPOX via the $\text{ISOPO}_2 + \text{HO}_2$ pathway. Although the three mechanisms agree better under high NO_x conditions, they show different pathways contributing to glyoxal production.

With the constraints from field measurements during SENEX, AM3ST with an effective reactive uptake coefficient γ_{glyx} of 2×10^{-3} and AM3B without heterogeneous loss of glyoxal can best reproduce the observed vertical profile. The latter shows better agreement with observed R_{GF} in the boundary layer. These two choices lead to less than $0.8 \mu\text{g m}^{-3}$ or negligible of glyoxal SOA in the boundary layer of the Southeast U.S., accounting for 0–14% of the total SOA in this region (Figure S7). These are likely the lower limit of glyoxal SOA due to other sources of glyoxal other than isoprene oxidation that are not included in our model. Over North America, glyoxal sinks are dominated by photolysis, followed by aerosol uptake and OH oxidation for AM3ST and OH oxidation and aerosol uptake for AM3B. Dry and wet deposition are much smaller than chemical loss for both AM3 versions (Table 1).

In the boundary layer, observations suggest a very similar NO_x dependence for HCHO and glyoxal, resulting in a nearly constant R_{GF} across NO_x levels [Kaiser *et al.*, 2015]. Both AM3ST and AM3B can roughly capture the NO_x dependence of HCHO and glyoxal, although AM3ST tends to overestimate R_{GF} at all NO_x regimes, likely due to the overestimate of glyoxal at low NO_x and underestimate of HCHO across NO_x regimes. AM3B shows a positive bias in R_{GF} at $\text{NO}_x < 0.5$ ppbv due to insufficient production of HCHO. The MCM v3.3.1-like mechanism (AM3M) shows a large underestimate of glyoxal across all NO_x levels. One possible reason is the lack of a radical propagating channel for the $\text{IEPOXOO} + \text{HO}_2$ reaction in MCM v3.3.1.

While glyoxal has been studied extensively over the past decade to understand the magnitude of its heterogeneous uptake, we show here that its gas-phase production is a large source of uncertainty that requires equal consideration. We find that its production from isoprene oxidation varies greatly among different chemical mechanisms. This in turn greatly impacts global estimates of glyoxal and in particular its contribution to SOA, especially in regions with low to moderate NO_x levels (Figure 1). Under high NO_x conditions, models differ significantly in the production of glyoxal from oxidation of glycolaldehyde, as well as the fate of $\delta\text{-ISOPO}_2$. Under low NO_x conditions, there is very little laboratory evidence available on the production of glyoxal from IEPOX, HPALDs, di-HPCARPs, or other intermediate products. Although heterogeneous loss of IEPOX is not included in the current work, sensitivity tests show that inclusion of this uptake reduces glyoxal concentrations by 10–20% for the mean vertical profile over the Southeast U.S. Thus, the fate of IEPOX represents another mechanistic uncertainty for predicting glyoxal. Also, there are missing sources not represented in our model [Baidar *et al.*, 2013; Lee *et al.*, 1998; Volkamer *et al.*, 2015] that would increase modeled glyoxal and thus also inferred SOA. Future laboratory measurements are urgently needed and may have important implications for understanding the contribution of glyoxal to SOA in past and future atmospheres.

References

- Anderson, D. C., *et al.* (2014), Measured and modeled CO and NO_y in DISCOVER-AQ: An evaluation of emissions and chemistry over the eastern US, *Atmos. Environ.*, 96, 78–87, doi:10.1016/j.atmosenv.2014.07.004.
- Baidar, S., H. Oetjen, S. Coburn, B. Dix, I. Ortega, R. Sinreich, and R. Volkamer (2013), The CU Airborne MAX-DOAS instrument: Vertical profiling of aerosol extinction and trace gases, *Atmos. Meas. Tech.*, 6(3), 719–739, doi:10.5194/amt-6-719-2013.

Acknowledgments

The authors thank Charles A. Brock (NOAA) for providing the aerosol size data, Vaishali Naik (UCAR/NOAA) for providing the emission inventories from the SENEX campaign, and William Cooke for the help with convection scheme of the AM3 model. J.L., J.M., and L.W.H. acknowledge supports by the NOAA Climate Program Office grant NA13OAR4310071 and NA14OAR4320106. K.E.M., R.A.W., and S.S. B. acknowledge the support from the NOAA Atmospheric Chemistry, Climate, and Carbon Cycle (AC4) program. J.K., F.N. K., G.M.W., and T.F.H. are grateful for the support from EPA Science to Achieve Results program grant 83540601 and NASA grant NNN10ZDA001N-SEAC4RS. J. Kaiser acknowledges support from NASA Headquarters under the NASA Earth and Space Science Fellowship Program grant NNX14AK97H. R.V. is grateful for the support from NSF EAGER award AGS-1452317. V.F.M. acknowledges support from NSF (AGS-1546136). We thank the staff at the NOAA Aircraft Operations Center and the WP-3D flight crew for their help in instrumenting the aircraft and for conducting the flights. Special thanks go to Songmiao Fan (NOAA) for the helpful discussions. This research has not been subjected to any EPA review and therefore does not necessarily reflect the views of the agency, and no official endorsement should be inferred. Observational data sets and modeling results are available upon request to the corresponding author (Jingqiu.Mao@noaa.gov).

- Bates, K. H., J. D. Crouse, J. M. St. Clair, N. B. Bennett, T. B. Nguyen, J. H. Seinfeld, B. M. Stoltz, and P. O. Wennberg (2014), Gas phase production and loss of isoprene epoxydiols, *J. Phys. Chem. A*, *118*(7), 1237–1246, doi:10.1021/JP4107958.
- Butkovskaya, N. I., N. Povesle, A. Kukui, and G. Le Bras (2006), Mechanism of the OH-initiated oxidation of glycolaldehyde over the temperature range 233–296 K, *J. Phys. Chem. A*, *110*(50), 13,492–13,499, doi:10.1021/JP064993k.
- Carlton, A. G., B. J. Turpin, K. E. Altieri, S. Seitzinger, A. Reff, H.-J. Lim, and B. Ervens (2007), Atmospheric oxalic acid and SOA production from glyoxal: Results of aqueous photooxidation experiments, *Atmos. Environ.*, *41*(35), 7588–7602, doi:10.1016/j.atmosenv.2007.05.035.
- Cazorla, M., G. M. Wolfe, S. A. Bailey, A. K. Swanson, H. L. Arkinson, and T. F. Hanisco (2015), A new airborne laser-induced fluorescence instrument for in situ detection of formaldehyde throughout the troposphere and lower stratosphere, *Atmos. Meas. Tech.*, *8*(2), 541–552, doi:10.5194/amt-8-541-2015.
- Chan Miller, C., G. Gonzalez Abad, H. Wang, X. Liu, T. Kurosu, D. J. Jacob, and K. Chance (2014), Glyoxal retrieval from the Ozone Monitoring Instrument, *Atmos. Meas. Tech.*, *7*(11), 3891–3907, doi:10.5194/amt-7-3891-2014.
- Ciobanu, V. G., C. Marcolli, U. K. Krieger, U. Weers, and T. Peter (2009), Liquid–liquid phase separation in mixed organic/inorganic aerosol particles, *J. Phys. Chem. A*, *113*(41), 10,966–10,978, doi:10.1021/JP905054d.
- Corrigan, A. L., S. W. Hanley, and D. O. De Haan (2008), Uptake of glyoxal by organic and inorganic aerosol, *Environ. Sci. Technol.*, *42*(12), 4428–4433, doi:10.1021/es7032394.
- Crouse, J. D., F. Paulot, H. G. Kjaergaard, and P. O. Wennberg (2011), Peroxy radical isomerization in the oxidation of isoprene, *Phys. Chem. Chem. Phys.*, *13*(30), 13,607–13,613, doi:10.1039/C1cp21330j.
- DiGangi, J. P., et al. (2012), Observations of glyoxal and formaldehyde as metrics for the anthropogenic impact on rural photochemistry, *Atmos. Chem. Phys.*, *12*(20), 9529–9543, doi:10.5194/acp-12-9529-2012.
- Dillon, T. J., and J. N. Crowley (2008), Direct detection of OH formation in the reactions of HO₂ with CH₃C(O)O₂ and other substituted peroxy radicals, *Atmos. Chem. Phys.*, *8*(16), 4877–4889, doi:10.5194/acp-8-4877-2008.
- Donner, L. J., et al. (2011), The dynamical core, physical parameterizations, and basic simulation characteristics of the atmospheric component AM3 of the GFDL global coupled model CM3, *J. Clim.*, *24*(13), 3484–3519, doi:10.1175/2011JCLI3955.1.
- Emmerson, K. M., and M. J. Evans (2009), Comparison of tropospheric gas-phase chemistry schemes for use within global models, *Atmos. Chem. Phys.*, *9*(5), 1831–1845, doi:10.5194/acp-9-1831-2009.
- Ervens, B., B. J. Turpin, and R. J. Weber (2011), Secondary organic aerosol formation in cloud droplets and aqueous particles (aqSOA): A review of laboratory, field and model studies, *Atmos. Chem. Phys.*, *11*(21), 11,069–11,102, doi:10.5194/acp-11-11069-2011.
- Feierabend, K. J., J. E. Flad, S. S. Brown, and J. B. Burkholder (2009), HCO quantum yields in the photolysis of HC(O)C(O)H (glyoxal) between 290 and 420 nm, *J. Phys. Chem. A*, *113*(27), 7784–7794, doi:10.1021/JP9033003.
- Fu, T.-M., D. J. Jacob, F. Wittrock, J. P. Burrows, M. Vrekoussis, and D. K. Henze (2008), Global budgets of atmospheric glyoxal and methylglyoxal, and implications for formation of secondary organic aerosols, *J. Geophys. Res.*, *113*, D15303, doi:10.1029/2007JD009505.
- Galloway, M. M., P. S. Chhabra, A. W. H. Chan, J. D. Surratt, R. C. Flagan, J. H. Seinfeld, and F. N. Keutsch (2009), Glyoxal uptake on ammonium sulphate seed aerosol: Reaction products and reversibility of uptake under dark and irradiated conditions, *Atmos. Chem. Phys.*, *9*(10), 3331–3345, doi:10.5194/acp-9-3331-2009.
- Galloway, M. M., A. J. Huisman, L. D. Yee, A. W. H. Chan, C. L. Loza, J. H. Seinfeld, and F. N. Keutsch (2011a), Yields of oxidized volatile organic compounds during the OH radical initiated oxidation of isoprene, methyl vinyl ketone, and methacrolein under high-NO_x conditions, *Atmos. Chem. Phys.*, *11*(21), 10,779–10,790, doi:10.5194/acp-11-10779-2011.
- Galloway, M. M., C. L. Loza, P. S. Chhabra, A. W. H. Chan, L. D. Yee, J. H. Seinfeld, and F. N. Keutsch (2011b), Analysis of photochemical and dark glyoxal uptake: Implications for SOA formation, *Geophys. Res. Lett.*, *38*, L17811, doi:10.1029/2011GL048514.
- Gaston, C. J., T. P. Riedel, Z. Zhang, A. Gold, J. D. Surratt, and J. A. Thornton (2014), Reactive uptake of an isoprene-derived epoxydiol to submicron aerosol particles, *Environ. Sci. Technol.*, *48*(19), 11,178–11,186, doi:10.1021/es5034266.
- Gomez, M. E., Y. Lin, S. Guo, and R. Zhang (2015), Heterogeneous chemistry of glyoxal on acidic solutions. An oligomerization pathway for secondary organic aerosol formation, *J. Phys. Chem. A*, *119*(19), 4457–4463, doi:10.1021/jp509916r.
- Guenther, A., T. Karl, P. Harley, C. Wiedinmyer, P. I. Palmer, and C. Geron (2006), Estimates of global terrestrial isoprene emissions using MEGAN (Model of Emissions of Gases and Aerosols from Nature), *Atmos. Chem. Phys.*, *6*(11), 3181–3210, doi:10.5194/acp-6-3181-2006.
- Hasson, A. S., G. S. Tyndall, and J. J. Orlando (2004), A product yield study of the reaction of HO₂ radicals with ethyl peroxy (C₂H₅O₂), acetyl peroxy (CH₃C(O)O₂), and acetonyl peroxy (CH₃C(O)CH₂O₂) radicals, *J. Phys. Chem. A*, *108*(28), 5979–5989, doi:10.1021/jp048873t.
- Hastings, W. P., C. A. Koehler, E. L. Bailey, and D. O. De Haan (2005), Secondary organic aerosol formation by glyoxal hydration and oligomer formation: Humidity effects and equilibrium shifts during analysis, *Environ. Sci. Technol.*, *39*(22), 8728–8735, doi:10.1021/es050446l.
- Hays, M. D., C. D. Geron, K. J. Linna, N. D. Smith, and J. J. Schauer (2002), Speciation of gas-phase and fine particle emissions from burning of foliar fuels, *Environ. Sci. Technol.*, *36*(11), 2281–2295, doi:10.1021/es0111683.
- Hudman, R. C., et al. (2007), Surface and lightning sources of nitrogen oxides over the United States: Magnitudes, chemical evolution, and outflow, *J. Geophys. Res.*, *112*, D12505, doi:10.1029/2006JD007912.
- Huijnen, V., J. E. Williams, and J. Flemming (2014), Modeling global impacts of heterogeneous loss of HO₂ on cloud droplets, ice particles and aerosols, *Atmos. Chem. Phys. Discuss.*, *14*, 8575–8632, doi:10.5194/acpd-14-8575-2014.
- Jacob, D. J. (2000), Heterogeneous chemistry and tropospheric ozone, *Atmos. Environ.*, *34*(12–14), 2131–2159, doi:10.1016/S1352-2310(99)00462-8.
- Jacobs, M. I., A. I. Darer, and M. J. Elrod (2013), Rate constants and products of the OH reaction with isoprene-derived epoxides, *Environ. Sci. Technol.*, *47*(22), 12,868–12,876, doi:10.1021/es403340g.
- Jang, M., N. M. Czoschke, S. Lee, and R. M. Kamens (2002), Heterogeneous atmospheric aerosol production by acid-catalyzed particle-phase reactions, *Science*, *298*(5594), 814–817, doi:10.1126/science.1075798.
- Jenkin, M. E., S. M. Saunders, and M. J. Pilling (1997), The tropospheric degradation of volatile organic compounds: A protocol for mechanism development, *Atmos. Environ.*, *31*(1), 81–104, doi:10.1016/S1352-2310(96)00105-7.
- Jenkin, M. E., M. D. Hurley, and T. J. Wallington (2007), Investigation of the radical product channel of the CH₃C(O)O₂ + HO₂ reaction in the gas phase, *Phys. Chem. Chem. Phys.*, *9*(24), 3149–3162, doi:10.1039/B702757E.
- Jenkin, M. E., J. C. Young, and A. R. Rickard (2015), The MCM v3.3.1 degradation scheme for isoprene, *Atmos. Chem. Phys.*, *15*(20), 11,433–11,459, doi:10.5194/acp-15-11433-2015.
- Kaiser, J., et al. (2015), Reassessing the ratio of glyoxal to formaldehyde as an indicator of hydrocarbon precursor speciation, *Atmos. Chem. Phys.*, *15*(13), 7571–7583, doi:10.5194/acp-15-7571-2015.
- Kampf, C. J., E. M. Waxman, J. G. Slowik, J. Dommen, L. Pfaffenberger, A. P. Praplan, A. S. H. Prévôt, U. Baltensperger, T. Hoffmann, and R. Volkamer (2013), Effective Henry's law partitioning and the salting constant of glyoxal in aerosols containing sulfate, *Environ. Sci. Technol.*, *47*(9), 4236–4244, doi:10.1021/es400083d.

- Knote, C., et al. (2014), Simulation of semi-explicit mechanisms of SOA formation from glyoxal in aerosol in a 3-D model, *Atmos. Chem. Phys.*, 14(12), 6213–6239, doi:10.5194/acp-14-6213-2014.
- Kroll, J. H., N. L. Ng, S. M. Murphy, V. Varutbangkul, R. C. Flagan, and J. H. Seinfeld (2005), Chamber studies of secondary organic aerosol growth by reactive uptake of simple carbonyl compounds, *J. Geophys. Res.*, 110, D23207, doi:10.1029/2005JD006004.
- Kurtén, T., J. Elm, N. L. Prisle, K. V. Mikkelsen, C. J. Kampf, E. M. Waxman, and R. Volkamer (2015), Computational study of the effect of glyoxal–sulfate clustering on the Henry's law coefficient of glyoxal, *J. Phys. Chem. A*, 119(19), 4509–4514, doi:10.1021/jp510304c.
- Lamarque, J. F., G. P. Kyle, M. Meinshausen, K. Riahi, S. Smith, D. van Vuuren, A. Conley, and F. Vitt (2011), Global and regional evolution of short-lived radiatively-active gases and aerosols in the Representative Concentration Pathways, *Clim. Change*, 109(1-2), 191–212, doi:10.1007/s10584-011-0155-0.
- Lee, L., A. P. Teng, P. O. Wennberg, J. D. Crounse, and R. C. Cohen (2014), On rates and mechanisms of OH and O₃ reactions with isoprene-derived hydroxy nitrates, *J. Phys. Chem. A*, 118(9), 1622–1637, doi:10.1021/jp4107603.
- Lee, Y. N., et al. (1998), Atmospheric chemistry and distribution of formaldehyde and several multioxygenated carbonyl compounds during the 1995 Nashville/Middle Tennessee Ozone Study, *J. Geophys. Res.*, 103(D17), 22,449–22,462, doi:10.1029/98JD01251.
- Li, J., M. Cleveland, L. D. Ziemba, R. J. Griffin, K. C. Barsanti, J. F. Pankow, and Q. Ying (2015), Modeling regional secondary organic aerosol using the Master Chemical Mechanism, *Atmos. Environ.*, 102, 52–61, doi:10.1016/j.atmosenv.2014.11.054.
- Liggio, J., S.-M. Li, and R. McLaren (2005a), Heterogeneous reactions of glyoxal on particulate matter: Identification of acetals and sulfate esters, *Environ. Sci. Technol.*, 39(6), 1532–1541, doi:10.1021/es048375y.
- Liggio, J., S.-M. Li, and R. McLaren (2005b), Reactive uptake of glyoxal by particulate matter, *J. Geophys. Res.*, 110, D10304, doi:10.1029/2004JD005113.
- Lim, H.-J., A. G. Carlton, and B. J. Turpin (2005), Isoprene forms secondary organic aerosol through cloud processing: Model simulations, *Environ. Sci. Technol.*, 39(12), 4441–4446, doi:10.1021/es048039h.
- Lin, M., et al. (2012), Transport of Asian ozone pollution into surface air over the western United States in spring, *J. Geophys. Res.*, 117, D00V07, doi:10.1029/2011JD016961.
- Lockwood, A. L., P. B. Shepson, M. N. Fiddler, and M. Alaghmand (2010), Isoprene nitrates: Preparation, separation, identification, yields, and atmospheric chemistry, *Atmos. Chem. Phys.*, 10(13), 6169–6178, doi:10.5194/acp-10-6169-2010.
- MacDonald, S. M., H. Oetjen, A. S. Mahajan, L. K. Whalley, P. M. Edwards, D. E. Heard, C. E. Jones, and J. M. C. Plane (2012), DOAS measurements of formaldehyde and glyoxal above a south-east Asian tropical rainforest, *Atmos. Chem. Phys.*, 12(13), 5949–5962, doi:10.5194/acp-12-5949-2012.
- Mao, J., et al. (2010), Chemistry of hydrogen oxide radicals (HO_x) in the Arctic troposphere in spring, *Atmos. Chem. Phys.*, 10(13), 5823–5838, doi:10.5194/acp-10-5823-2010.
- Mao, J., L. W. Horowitz, V. Naik, S. Fan, J. Liu, and A. M. Fiore (2013a), Sensitivity of tropospheric oxidants to biomass burning emissions: Implications for radiative forcing, *Geophys. Res. Lett.*, 40, 1241–1246, doi:10.1002/grl.50210.
- Mao, J., F. Paulot, D. J. Jacob, R. C. Cohen, J. D. Crounse, P. O. Wennberg, C. A. Keller, R. C. Hudman, M. P. Barkley, and L. W. Horowitz (2013b), Ozone and organic nitrates over the eastern United States: Sensitivity to isoprene chemistry, *J. Geophys. Res. Atmos.*, 118, 11,256–11,268, doi:10.1002/jgrd.50817.
- Marais, E. A., et al. (2016), Aqueous-phase mechanism for secondary organic aerosol formation from isoprene: Application to the Southeast United States and co-benefit of SO₂ emission controls, *Atmos. Chem. Phys.*, 16(3), 1603–1618, doi:10.5194/acp-16-1603-2016.
- Millet, D. B., D. J. Jacob, K. F. Boersma, T.-M. Fu, T. P. Kurosu, K. Chance, C. L. Heald, and A. Guenther (2008), Spatial distribution of isoprene emissions from North America derived from formaldehyde column measurements by the OMI satellite sensor, *J. Geophys. Res.*, 113, D02307, doi:10.1029/2007JD008950.
- Min, K. E., et al. (2016), A broadband cavity enhanced absorption spectrometer for aircraft measurements of glyoxal, methylglyoxal, nitrous acid, nitrogen dioxide, and water vapor, *Atmos. Meas. Tech.*, 9(2), 423–440, doi:10.5194/amt-9-423-2016.
- Müller, J. F., J. Peeters, and T. Stavrou (2014), Fast photolysis of carbonyl nitrates from isoprene, *Atmos. Chem. Phys.*, 14(5), 2497–2508, doi:10.5194/acp-14-2497-2014.
- Myriokefalitakis, S., M. Vrekoussis, K. Tsigaridis, F. Wittrock, A. Richter, C. Brühl, R. Volkamer, J. P. Burrows, and M. Kanakidou (2008), The influence of natural and anthropogenic secondary sources on the glyoxal global distribution, *Atmos. Chem. Phys.*, 8(16), 4965–4981, doi:10.5194/acp-8-4965-2008.
- Naik, V., L. W. Horowitz, A. M. Fiore, P. Ginoux, J. Mao, A. M. Aghedo, and H. Levy (2013), Impact of preindustrial to present-day changes in short-lived pollutant emissions on atmospheric composition and climate forcing, *J. Geophys. Res. Atmos.*, 118, 8086–8110, doi:10.1002/jgrd.50608.
- Nguyen, T. B., J. D. Crounse, A. P. Teng, J. M. S. Clair, F. Paulot, G. M. Wolfe, and P. O. Wennberg (2015), Rapid deposition of oxidized biogenic compounds to a temperate forest, *Proc. Natl. Acad. Sci. U.S.A.*, 112(5), E392–E401, doi:10.1073/pnas.1418702112.
- Niki, H., P. D. Maker, C. M. Savage, and M. D. Hurley (1987), Fourier transform infrared study of the kinetics and mechanisms for the chlorine-atom- and hydroxyl-radical-initiated oxidation of glycolaldehyde, *J. Phys. Chem.*, 91(8), 2174–2178, doi:10.1021/J100292a038.
- Nozière, B., P. Dziedzic, and A. Córdoba (2009), Products and kinetics of the liquid-phase reaction of glyoxal catalyzed by ammonium ions (NH₄⁺), *J. Phys. Chem. A*, 113(1), 231–237, doi:10.1021/jp8078293.
- Palmer, P. I., D. J. Jacob, A. M. Fiore, R. V. Martin, K. Chance, and T. P. Kurosu (2003), Mapping isoprene emissions over North America using formaldehyde column observations from space, *J. Geophys. Res.*, 108(D6), 4180, doi:10.1029/2002JD002153.
- Paulot, F., J. D. Crounse, H. G. Kjaergaard, J. H. Kroll, J. H. Seinfeld, and P. O. Wennberg (2009a), Isoprene photooxidation: New insights into the production of acids and organic nitrates, *Atmos. Chem. Phys.*, 9(4), 1479–1501, doi:10.5194/acp-9-1479-2009.
- Paulot, F., J. D. Crounse, H. G. Kjaergaard, A. Kürten, J. M. S. Clair, J. H. Seinfeld, and P. O. Wennberg (2009b), Unexpected epoxide formation in the gas-phase photooxidation of isoprene, *Science*, 325(5941), 730–733, doi:10.1126/science.1172910.
- Paulot, F., P. Ginoux, W. F. Cooke, L. J. Donner, S. Fan, M. Y. Lin, J. Mao, V. Naik, and L. W. Horowitz (2016), Sensitivity of nitrate aerosols to ammonia emissions and to nitrate chemistry: Implications for present and future nitrate optical depth, *Atmos. Chem. Phys.*, 16(3), 1459–1477, doi:10.5194/acp-16-1459-2016.
- Peeters, J., and T. L. Nguyen (2012), Unusually fast 1,6-H shifts of enolic hydrogens in peroxy radicals: Formation of the first-generation C₂ and C₃ carbonyls in the oxidation of isoprene, *J. Phys. Chem. A*, 116(24), 6134–6141, doi:10.1021/jp211447q.
- Peeters, J., J.-F. Müller, T. Stavrou, and V. S. Nguyen (2014), Hydroxyl radical recycling in isoprene oxidation driven by hydrogen bonding and hydrogen tunneling: The upgraded LIM1 mechanism, *J. Phys. Chem. A*, 118(38), 8625–8643, doi:10.1021/jp5033146.
- Praske, E., J. D. Crounse, K. H. Bates, T. Kurtén, H. G. Kjaergaard, and P. O. Wennberg (2015), Atmospheric fate of methyl vinyl ketone: Peroxy radical reactions with NO and HO₂, *J. Phys. Chem. A*, 119(19), 4562–4572, doi:10.1021/jp5107058.
- Pye, H. O. T., et al. (2013), Epoxide pathways improve model predictions of isoprene markers and reveal key role of acidity in aerosol formation, *Environ. Sci. Technol.*, 47(19), 11,056–11,064, doi:10.1021/es402106h.

- Rivera-Rios, J. C., et al. (2014), Conversion of hydroperoxides to carbonyls in field and laboratory instrumentation: Observational bias in diagnosing pristine versus anthropogenically controlled atmospheric chemistry, *Geophys. Res. Lett.*, *41*, 8645–8651, doi:10.1002/2014GL061919.
- Sander, R. (2015), Compilation of Henry's law constants (version 4.0) for water as solvent, *Atmos. Chem. Phys.*, *15*(8), 4399–4981, doi:10.5194/acp-15-4399-2015.
- Saunders, S. M., M. E. Jenkin, R. G. Derwent, and M. J. Pilling (2003), Protocol for the development of the Master Chemical Mechanism, MCM v3 (Part A): Tropospheric degradation of non-aromatic volatile organic compounds, *Atmos. Chem. Phys.*, *3*(1), 161–180, doi:10.5194/acp-3-161-2003.
- St. Clair, J. M., J. C. Rivera-Rios, J. D. Crouse, H. C. Knap, K. H. Bates, A. P. Teng, S. Jørgensen, H. G. Kjaergaard, F. N. Keutsch, and P. O. Wennberg (2016a), Kinetics and products of the reaction of the first-generation isoprene hydroxy hydroperoxide (ISOPPOH) with OH, *J. Phys. Chem. A*, *120*(9), 1441–1451, doi:10.1021/acs.jpca.5b06532.
- St. Clair, J. M., J. C. Rivera-Rios, J. D. Crouse, E. Praske, M. J. Kim, G. M. Wolfe, F. N. Keutsch, P. O. Wennberg, and T. F. Hanisco (2016b), Investigation of a potential HCHO measurement artifact from ISOPPOH, *Atmos. Meas. Tech. Discuss.*, *2016*, 1–15, doi:10.5194/amt-2016-204.
- Stavrakou, T., J. F. Müller, I. De Smedt, M. Van Roozendaal, M. Kanakidou, M. Vrekoussis, F. Wittrock, A. Richter, and J. P. Burrows (2009), The continental source of glyoxal estimated by the synergistic use of spaceborne measurements and inverse modelling, *Atmos. Chem. Phys.*, *9*(21), 8431–8446, doi:10.5194/acp-9-8431-2009.
- Stavrakou, T., J. Peeters, and J. F. Müller (2010), Improved global modelling of HO_x recycling in isoprene oxidation: Evaluation against the GABRIEL and INTEX-A aircraft campaign measurements, *Atmos. Chem. Phys.*, *10*(20), 9863–9878, doi:10.5194/acp-10-9863-2010.
- Teng, A. P., J. D. Crouse, L. Lee, J. M. St. Clair, R. C. Cohen, and P. O. Wennberg (2015), Hydroxy nitrate production in the OH-initiated oxidation of alkenes, *Atmos. Chem. Phys.*, *15*(8), 4297–4316, doi:10.5194/acp-15-4297-2015.
- Travis, K., et al. (2015), Declining NO_x in the Southeast US and implications for ozone-NO_x-VOC chemistry, in *SEAC⁴RS Science Team Meeting*, edited, Pasadena, California.
- Volkamer, R., L. T. Molina, M. J. Molina, T. Shirley, and W. H. Brune (2005), DOAS measurement of glyoxal as an indicator for fast VOC chemistry in urban air, *Geophys. Res. Lett.*, *32*, L08806, doi:10.1029/2005GL022616.
- Volkamer, R., I. Barnes, U. Platt, L. T. Molina, and M. J. Molina (2006), Remote sensing of glyoxal by differential optical absorption spectroscopy (DOAS): Advancements in simulation chamber and field experiments, in *Environmental Simulation Chambers: Application to Atmospheric Chemical Processes*, edited by I. Barnes and K. Rudzinski, pp. 129–141, Springer, Netherlands, doi:10.1007/1-4020-4232-9_10.
- Volkamer, R., F. San Martini, L. T. Molina, D. Salcedo, J. L. Jimenez, and M. J. Molina (2007), A missing sink for gas-phase glyoxal in Mexico City: Formation of secondary organic aerosol, *Geophys. Res. Lett.*, *34*, L19807, doi:10.1029/2007GL030752.
- Volkamer, R., P. J. Ziemann, and M. J. Molina (2009), Secondary organic aerosol formation from acetylene (C₂H₂): Seed effect on SOA yields due to organic photochemistry in the aerosol aqueous phase, *Atmos. Chem. Phys.*, *9*(6), 1907–1928, doi:10.5194/acp-9-1907-2009.
- Volkamer, R., et al. (2015), Aircraft measurements of BrO, IO, glyoxal, NO₂, H₂O, O₂–O₂ and aerosol extinction profiles in the tropics: Comparison with aircraft-/ship-based in situ and lidar measurements, *Atmos. Meas. Tech.*, *8*(5), 2121–2148, doi:10.5194/amt-8-2121-2015.
- Vrekoussis, M., F. Wittrock, A. Richter, and J. P. Burrows (2010), GOME-2 observations of oxygenated VOCs: What can we learn from the ratio glyoxal to formaldehyde on a global scale? *Atmos. Chem. Phys.*, *10*(21), 10,145–10,160, doi:10.5194/acp-10-10145-2010.
- Warneke, C., et al. (2010), Biogenic emission measurement and inventories determination of biogenic emissions in the eastern United States and Texas and comparison with biogenic emission inventories, *J. Geophys. Res.*, *115*, D00F18, doi:10.1029/2009JD012445.
- Warneke, C., et al. (2016), Instrumentation and measurement strategy for the NOAA SENEX aircraft campaign as part of the Southeast Atmosphere Study 2013, *Atmos. Meas. Tech.*, *9*(7), 3063–3093, doi:10.5194/amt-9-3063-2016.
- Washenfelder, R. A., et al. (2011), The glyoxal budget and its contribution to organic aerosol for Los Angeles, California, during CalNex 2010, *J. Geophys. Res.*, *116*, D00V02, doi:10.1029/2011JD016314.
- Waxman, E. M., J. Elm, T. Kurtén, K. V. Mikkelsen, P. J. Ziemann, and R. Volkamer (2015), Glyoxal and methylglyoxal Setschenow salting constants in sulfate, nitrate, and chloride solutions: Measurements and Gibbs energies, *Environ. Sci. Technol.*, *49*(19), 11,500–11,508, doi:10.1021/acs.est.5b02782.
- Wolfe, G. M., et al. (2016), Formaldehyde production from isoprene oxidation across NO_x regimes, *Atmos. Chem. Phys.*, *16*(4), 2597–2610, doi:10.5194/acp-16-2597-2016.
- Xiong, F., et al. (2015), Observation of isoprene hydroxynitrates in the southeastern United States and implications for the fate of NO_x, *Atmos. Chem. Phys.*, *15*(19), 11,257–11,272, doi:10.5194/acp-15-11257-2015.
- Ying, Q., J. Li, and S. H. Kota (2015), Significant contributions of isoprene to summertime secondary organic aerosol in eastern United States, *Environ. Sci. Technol.*, *49*(13), 7834–7842, doi:10.1021/acs.est.5b02514.
- Zhao, J., N. P. Levitt, R. Zhang, and J. Chen (2006), Heterogeneous reactions of methylglyoxal in acidic media: Implications for secondary organic aerosol formation, *Environ. Sci. Technol.*, *40*(24), 7682–7687, doi:10.1021/es060610k.